PERGAMON

International Journal of Heat and Mass Transfer 42 (1999) 111–126

International Journal of HEAT and MASS TRANSFER

Convection induced by residual-g and g-jitters in diffusion experiments

R. Savino*, R. Monti

Università degli Studi di Napoli 'Federico II', Dipartimento di Scienza e Ingegneria dello Spazio, 'L. G. Napolitano', P. le V. Tecchio 80, 80125 Napoli, Italy

Received 4 April 1997; in final form 31 March 1998

Abstract

Natural and vibrational convection induced by steady residual-g and high frequency g-jitters is studied in a typical process for the measurement of the diffusion coefficients in liquids at isothermal conditions on orbiting platforms. The averaged field equations are derived in the general case of a binary mixture with simultaneous heat/mass transfer, but the particular case of an isothermal mixture is considered to analyse the concentration distortions induced by g-disturbances during the diffusion experiment. The non-dimensional equations, subjected to appropriate initial and boundary conditions, are numerically integrated for different residual-g levels and g-jitters. The time profiles of the concentration distortions and the percentage errors in the measurement of the diffusion coefficient are reported for different values of the solutal gravitational Peclet number (Pe_g) for residual-g only without any g-jitter, for different solutal vibrational Peclet numbers (Pe_v) for g-jitters only without residual-g, and in the combined case of simultaneous residual-g and g-jitters. As a practical application, the tolerability domains in the plane (frequency, acceleration) are obtained in correspondence of a maximum allowed percentage error.

Nomenclature

b amplitude of the sinusoidal displacement
c mass concentration
c' pulsating part of the concentration
c_{diff} concentration in the diffusive (zero-g) field
c_m average part of the concentration
C Cross-average concentration
D mass diffusion coefficient
D_{diff} diffusion coefficient in the ideal (zero-g) situation
$\mathbf{g}$ gravity acceleration
$\mathbf{g}_s$ steady residual g-level
$\mathbf{g}_0$ Earth gravity acceleration
G amplitude of the oscillatory g-disturbances scaled by the Earth gravity acceleration
G_{max} maximum allowable g-level scaled by the earth gravity acceleration
G_s residual-g level scaled by the Earth gravity acceleration
H vertical length (along y)
L horizontal length (along x)
$\mathbf{n}$ unit vector of the vibration axis
p pressure
p' pulsating part of the pressure
p_m average part of the pressure
P_{err} percentage error in the measurement of diffusion coefficient
Pe_g gravitational Peclet number
Pe_v vibrational Peclet number
Pr Prandtl number
$\mathbf{r}$ position vector at the boundary
Sc Schmidt number
t time
T temperature
T' pulsating part of the temperature
T_m average part of the temperature
u, v velocity components along x, y directions
$\mathbf{V}$ velocity vector
$\mathbf{V}'$ pulsating part of the velocity
$\mathbf{V}_m$ average part of the velocity
w_1, w_2 components of the vector $\mathbf{w}$ along x, y directions
$\mathbf{w}$ solenoidal part of $(\beta_T T+\beta_c c)\mathbf{n}$
x, y Cartesian coordinates.

* Corresponding author.

0017–9310/98 $19.00
PII: S0017–9310(98)00140–9

Greek symbols

α thermal diffusivity
β_c solutal expansion coefficient
β_T thermal expansion coefficient
ΔC imposed concentration difference
ΔT imposed temperature difference
Δ_2 Laplace operator
ε_c concentration distortion
μ dynamic viscosity
ν kinematic viscosity
ρ density
φ potential of $T\mathbf{n}$
ω angular velocity of the sinusoidal g-disturbance
∇ Nabla operator.

1. Introduction

Experience has shown that available microgravity platforms (sounding rockets, Spacelab, Eureca, MIR, etc.) are not ideally free falling or free orbiting platforms (so they cannot give zero gravity). Systematic characterisation of the accelerations aboard space platforms have shown that the microgravity environment is dynamic, depending on many sources, e.g. aerodynamic forces, gravity gradient, solar pressure, attitude control actuation, on-board machinery, crew operations, servicing activities, docking/berthing, etc. [1–3].

The steady or quasi steady forces are responsible for 'residual-g'. Other time-dependent forces (impulsive, periodic) are responsible for 'g-jitter'.

It is recognised that the presence of g-disturbances may cause strong discrepancies in comparison with 'ideal zero-g' expected results; in fact the thermo-fluid-dynamic field of typical material and fluid science processes, based on purely diffusion-controlled conditions, may be substantially changed by g-disturbances.

The microgravity environment provides the means to drastically reduce convective contributions and thus to precisely determine diffusion properties of liquids [4]. However relevant distortions of the thermal and concentration fields, in comparison with purely diffusion conditions, may be caused by buoyant and average vibrational forces associated, respectively, to steady residual g-levels and g-jitters.

Since in many practical cases the acceleration field on the experimental test-cells is time-dependent, previous analyses of the effect of g-jitter on cavity flow have considered acceleration fields that are either periodic in time or a sequence of isolated pulses of short duration [5–8].

The influence of average vibrational convection induced by high frequency oscillations has been considered in the past by Richardson [9], who reviewed the effects of sound and wall vibration on heat transfer. Gershuni and Zukhovitsky [10] obtained the equations of vibro-convective motion in the closed form with boundary conditions, for a homogeneous fluid in a vibrating cell in presence of a temperature gradient. In more recent developments the order of magnitude analysis of these equations has been applied to the evaluation of the tolerability limits of microgravity experiments [11, 12]. Further numerical application studies on the subject have been published in [13, 18].

In this paper the average equations are extended to the case of simultaneous temperature and concentration gradients in order to derive a general mathematical tool able to cope with a wide range of practical applications. As a first application the equations are numerically solved for a typical diffusion experiment envisioned for the measurement of the diffusion coefficients in liquids at isothermal conditions.

The paper runs as follows. A mathematical model is developed in the general case of a binary mixture with simultaneous temperature and concentration gradients. Then, the particular case of a binary isothermal mixture is considered and the non-dimensional equations, subjected to appropriate initial and boundary conditions, are numerically integrated with a finite-volume formulation explicit in time. The results pertaining to different residual-g levels and g-jitters are presented and discussed in terms of stream-lines, vector plots and concentration distributions. As a practical application, the tolerability domain in the plane (frequency, acceleration) is obtained in correspondence of a maximum allowed percentage error.

It must be pointed out that, although the case under investigation is isothermal, so that the energy equation is not solved, the general model here developed can be useful for simulations of similar applications when both energy and mass concentration diffusions are present (e.g. for experiments for the measurement of the Soret coefficient).

2. Averaged equations for simultaneous heat and mass transfer

We assume that the fluid system is subjected to a number of stimuli (imposed temperature and/or concentration differences), as well as to the gravitational forces representing the disturbances of the zero-g condition. The fluid is supposed homogeneous and Newtonian, with constant diffusion coefficients; the Boussinesq approximation applies for density; viscous dissipation is negligible.

Under the above hypotheses the flow is governed by the continuity, Navier–Stokes, energy and solute mass equations:

$$\nabla\cdot\mathbf{V}=0 \tag{1}$$

$$\mathbf{V}_t+\mathbf{V}\cdot\nabla\mathbf{V}+\frac{1}{\rho_r}\nabla p=\nu\Delta_2\mathbf{V}+\frac{(\rho-\rho_r)}{\rho_r}\mathbf{g}(t) \tag{2}$$

$$T_t+\mathbf{V}\cdot\nabla T=\alpha\Delta_2 T \tag{3}$$

$$c_t+\mathbf{V}\cdot\nabla c=D\Delta_2 c \tag{4}$$

where $\mathbf{g}(t)$ is the overall body force, per unit mass, ν, α and D are the kinematic viscosity, the thermal diffusivity and the diffusion coefficient, subscript 't' denotes partial derivation with respect to time and Δ_2 is the Laplace operator. The density is assumed to be a linear function of the temperature and of the concentration:

$$\rho=\rho_r[1-\beta_T(T-T_r)-\beta_c(c-c_r)] \tag{5}$$

where ρ_r is the density as the reference temperature T_r and at the reference concentration c_r, and β_T, β_c are the coefficients of expansion with temperature and concentration.

At the fluid cell boundaries a sinusoidal motion is applied, so that the position vector $\mathbf{r}$ on the boundary is a sinusoidal function of time:

$$\mathbf{r}(t)=b\cos(\omega t)\mathbf{n}. \tag{6}$$

This gives rise to a velocity and acceleration:

$$\mathbf{V}(t)=-b\omega\sin(\omega t)\mathbf{n} \tag{7}$$

$$\mathbf{g}_\omega(t)=-b\omega^2\cos(\omega t)\mathbf{n}. \tag{8}$$

In general a residual (steady) acceleration field $\mathbf{g}_S$ can be superimposed, so that the overall body force is:

$$\mathbf{g}(t)=\mathbf{g}_s-b\omega^2\cos(\omega t)\mathbf{n}. \tag{9}$$

The time-averaged model developed by Gershuni in the case of a single-component fluid subject to monochromatic vibration is extended to the case of simultaneous temperature and concentration gradients.

Under the assumptions that the vibration period is much less than the characteristic energy and mass diffusion times and that the amplitude of the oscillation is very small each thermo-fluid-dynamic variable can be separated into a pulsating component (with frequency ω) and a time-averaged part (over times much larger than ω^{-1}).

Taking the average of the (1a–d) over a period one obtains:

$$\nabla\cdot\mathbf{V}=0 \tag{10}$$

$$\mathbf{V}_t+\mathbf{V}\cdot\nabla\mathbf{V}+\overline{\mathbf{V}'\cdot\nabla\mathbf{V}'}+\frac{1}{\rho_r}\nabla p = \nu\Delta_2\mathbf{V}+b\omega^2\overline{(\beta_T T'+\beta_c c')\cos(\omega t)}\mathbf{n} \tag{11}$$

$$T_t+\mathbf{V}\cdot\nabla T+\overline{\mathbf{V}'\cdot\nabla T'}=\alpha\Delta_2 T \tag{12}$$

$$c_t+\mathbf{V}\cdot\nabla c+\overline{\mathbf{V}'\cdot\nabla c'}=D\Delta_2 c. \tag{13}$$

For the pulsating flow the momentum equation is obtained retaining only the time-dependent term, the pressure term and the 'linearized' driving term (convective and diffusive terms are neglected):

$$\mathbf{V}'_t+\frac{1}{\rho_r}\nabla p'=b\omega^2(\beta_T T+\beta_c c)\cos(\omega t)\mathbf{n}. \tag{14}$$

The equations for the temperature and concentration fluctuation read:

$$T'_t+\mathbf{V}'\cdot\nabla T=0 \tag{15}$$

$$c'_t+\mathbf{V}'\cdot\nabla c=0. \tag{16}$$

If the vector $(\beta_T T+\beta_c c)\mathbf{n}$ is expressed as:

$$(\beta_T T+\beta_c c)\mathbf{n}=\mathbf{w}+\nabla\varphi \tag{17}$$

with

$$\nabla\cdot\mathbf{w}=0 \tag{18}$$

$$\nabla\wedge\mathbf{w}=\nabla(\beta_T T+\beta_c c)\wedge\mathbf{n} \tag{19}$$

equation (14) can be separated into two equations (for the potential and the solenoidal parts):

$$\mathbf{V}'_t=b\omega^2\mathbf{w}\cos(\omega t) \tag{20}$$

$$\frac{1}{\rho_r}\nabla p'=b\omega^2\nabla\varphi\cos(\omega t). \tag{21}$$

Integration with respect to time of the (20) ($\mathbf{w}$ is not a function of time) yields:

$$\mathbf{V}'=b\omega\mathbf{w}\sin(\omega t) \tag{22}$$

that, substituted into the equations (15) and (16), gives:

$$T'_t+b\omega\sin(\omega t)\mathbf{w}\cdot\nabla T=0 \tag{23}$$

$$c'_t+b\omega\sin(\omega t)\mathbf{w}\cdot\nabla c=0. \tag{24}$$

Integration of the equations (23) and (24) gives:

$$T'=b\cos(\omega t)\mathbf{w}\cdot\nabla T \tag{25}$$

$$c'=b\cos(\omega t)\mathbf{w}\cdot\nabla c. \tag{26}$$

Equations (22), (25) and (26) can be used to evaluate the averaged values over an integer number of periods $(2\pi/\omega)$:

Substitution into the averaged equations and evaluation of the averaged values ($\overline{\mathbf{V}'\cdot\nabla C'}=0$; $\overline{\mathbf{V}'\cdot\nabla T'}=0$) lead to the following final system:

$$\nabla\cdot\mathbf{V}=0 \tag{27}$$

$$\mathbf{V}_t+\mathbf{V}\cdot\nabla\mathbf{V}+\frac{1}{\rho_r}\nabla p=\nu\Delta_2\mathbf{V}+\tfrac{1}{2}(b\omega)^2[\mathbf{w}\cdot\nabla(\beta_T T+\beta_c c)\mathbf{n}-\mathbf{w}\cdot\nabla\mathbf{w}] \tag{28}$$

$$T_t+\mathbf{V}\cdot\nabla T=\alpha\Delta_2 T \tag{29}$$

$$c_t+\mathbf{V}\cdot\nabla c=D\Delta_2 c \tag{30}$$

$$\nabla\cdot\mathbf{w}=0 \tag{31}$$

$$\nabla\wedge\mathbf{w}=\nabla(\beta_T T+\beta_C C)\wedge\mathbf{n}. \tag{32}$$

3. Idealised model of the diffusion experiment

A two-dimensional cell, of aspect ratio $A=L/H=4$, is filled with liquid and separated in two parts by a diaphragm. The diaphragm is located at distance $L/2$ from the walls along the horizontal direction. At the two sides

of the diaphragm the liquid contains different concentrations of the diffusing species. The direction of the g-jitters is the same as the residual gravity vector, that is oriented normally to the cell and directed downward. The cell is supposed to be at isothermal conditions. The side-walls are supposed to be adiabatic and there are no mass fluxes. The initial conditions at the beginning of the diffusion process (in the liquid phase) are prescribed. At time $t = 0$ the diaphragm is eliminated and the diffusion process takes place. A concentration profile will evolve with time in both sides of the cell. At steady state the concentration attains a constant value along x and y direction (equal to the average value of the initial concentrations at the two sides of the diaphragm).

In zero-g the concentration distribution at each time is one dimensional and the value of the diffusion coefficient can be correlated with the time profile of the concentration distribution along the ampoule. In particular, since the concentration gradient can be determined by differential interferograms, a practical method for the evaluation of the diffusion coefficient may be based on the observation, at given times, of the average concentration gradient along the longitudinal direction of the enclosure [19].

If the residual g is not zero or if g-jitters are applied, the concentration field is distorted and the accuracy of the measurement of the diffusion coefficient could be greatly affected.

The experiment under investigation is an idealization of a microgravity experiment on liquid–liquid diffusion. Similar experiments were performed by Littke during the first sounding rocket missions and in the Spacelab 1 [20, 21]. The experiment facility consists of two cylindrical container blocks, filled by miscible liquids with different initial concentrations, separated by a cylindrical glass plug which also contains one of the two liquids. The diffusion process begins when the plug is slowly rotated by 90°, so that the two chambers, initially isolated, become contiguous. The same concept has been recently applied to the crystallization reactors in the Advanced Protein Crystallization Facility developed by the European Space Agency as a standard tool for microgravity experiments aboard the NASA Space Shuttle and on the future International Space Station [22]. Flow perturbations at the initial stage of the process are reduced if the angular velocity of the plug is sufficiently small. Other technical solutions for these experiments are possible, for example two contiguous plates with holes initially misaligned, that move with a very small relative velocity until the holes correspond, leading the different liquids into contact. In particular, the technical solution that is being considered and that better simulates the one dimensional diffusive process consists in two adjacent nets (separating the two chambers) between which an impermeable thin foil is placed. This foil is withdrawn at the beginning of the experiment; this set up does not practically induce convective motions inside the two chambers.

4. Non-dimensional equations and boundary conditions

Equations (27)–(32), in the particular case $\nabla T = 0$, have been written in non-dimensional form in a Cartesian reference system using H^2/D, H, D/H, $\rho D^2/H^2$ and $\Delta c = c_2 - c_1$ to scale the time, the lengths, the velocity, the pressure and solute concentration (u, v and w_1, w_2 are the components of $\mathbf{V}$ and $\mathbf{w}$ along the x, y co-ordinates):

$$u_x + v_y = 0 \tag{33}$$

$$u_t + uu_x + vu_y + p_x = Sc(u_{xx} + u_{yy}) - Sc\,Pe_v\,[(w_1 w_1)_x + (w_1 w_2)_y] \tag{34}$$

$$v_t + uv_x + vv_y + p_y = Sc(v_{xx} + v_{yy}) - Sc\,Pe_g\,c - Sc\,Pe_v\,[(w_1 w_2 - w_1 c)_x + (w_2 w_2 - w_2 c)_y] \tag{35}$$

$$c_t + uc_x + vc_y = (c_{xx} + c_{yy}) \tag{36}$$

$$w_{1x} + w_{2y} = 0 \tag{37}$$

$$w_{2x} - w_{1y} = c_x \tag{38}$$

where:

$$Pe_g = \frac{g\beta_C \Delta c H^3}{vD} \quad Pe_v = \frac{(b\omega\beta_c \Delta c)^2 H^2}{2vD} \tag{39}$$

and Sc is the Schmidt number ($Sv = v/D$).

The choice for the reference time (H^2/D) and for the reference velocity (D/H) is motivated by the fact that the reference situation here is the purely diffusive one, corresponding to ideal zero-g conditions, in the absence of any residual-g or g-jitter. Convection arising from steady acceleration disturbances (residual-g) or by fluctuation of the acceleration (g-jitter) must be considered as a perturbation of the ideal reference state. Therefore the primary objective of this investigation is the evaluation of the convection-induced distortions in the concentration fields, since these perturbations affect the measured value of the diffusion coefficient.

With these scales the dimensionless parameters (39) can be interpreted as the ratios between the buoyancy [$V_g = g\beta_c \Delta c H^2/v$] or the vibrational [$V_v = (b\omega\beta_c \Delta c)^2 H/2v$] speed to the characteristic molecular diffusion speed (D/H) and therefore they are referred to as solutal gravitational or vibrational Peclet numbers, respectively ($V_g H/D$ and $V_v H/D$).

In some other literature these numbers are also referred to as solutal Rayleigh numbers (gravitational or vibrational). Similarly, the so-called Grashof numbers, defined by the ratio between the buoyant and the viscous speed, can be interpreted as Reynolds numbers, since they compare the relative importance between convection and viscous effects in the momentum equation, when the prevailing driving action is the buoyancy. For a more

general classification and discussion of these numbers see also [23, 24].

The Schmidt number ($Sc = v/D$) can be interpreted as the ratio between the characteristic mass diffusion and viscous times. In view of the large values of the solutal Peclet numbers (see following sections) the inertia terms in the equations (34, 35) must be necessarily taken into account, so that the Navier–Stokes equations must be numerically solved without any additional simplification. The fact that the Schmidt number is particularly large ($Sc = 690$, see following sections) means that the characteristic relaxation time in the concentration equation is larger than the viscous diffusion time, so that distortions of the concentration field exhibit long decay times also after the damping of the g-disturbances.

The initial and boundary conditions are:

4.1. Initial conditions

$$t = 0: \quad u = 0, \quad v = 0, \quad c = 1 \quad \text{for} \quad x < A/2 \quad \text{and} \quad c = 0 \quad \text{for} \quad x > A/2. \tag{40}$$

4.2. Boundary conditions

$$u(0, y) = u(A, y) = u(x, 0) = u(x, 1) = 0 \tag{41}$$

$$v(0, y) = v(A, y) = v(x, 0) = v(x, 1) = 0 \tag{42}$$

$$c_x(0, y) = c_x(A, y) = c_y(x, 0) = c_y(x, 1) = 0. \tag{43}$$

For the vector field **w** the homogeneous initial boundary conditions must be imposed.

The problem was solved numerically with the numerical method of control-volumes by a modified MAC method explicit in time. The domain was discretized with a staggered grid and the field equations, in the primitive variables (u, v, p), were numerically integrated using a classical second-order central scheme for the diffusive terms and a quadratic interpolation upwind method for the convective terms.

5. Results and discussion

In all the numerical calculations the following parameters have been considered: $L = 4$ cm, $H = 1$ cm, and $\Delta c = 1$.

The fluid was assumed to be an aqueous solution, with the following physical properties:

$$D = 1.5 \cdot 10^{-5}\ \mathrm{cm^2\ s^{-1}},$$

$$v = 10^{-2}\ \mathrm{cm^2\ s^{-1}}, \quad \beta_C = 10^{-2}, \quad Sc = 690.$$

The numerical results are presented and discussed in terms of stream-lines, vector plots, isoconcentration lines and concentration profiles. The solutal distortions, i.e. the differences of the concentration field with respect to the ideal zero-g field, are reported as functions of the solutal Peclet number (Pe_g), for residual (steady) g, and of the vibrational solutal Peclet number (Pe_v), for high frequency g-jitters, i.e. of the characteristic numbers measuring the relative importance of convective and diffusive effects in the solute transport equation.

5.1. Velocity and concentration fields

In Fig. 2 the streamlines 2(a), the vector plots 2(b) and the concentration distributions 2(c) are shown in the transient phase, for $Pe_v = 0$ (no g-jitters) and $Pe_g = 100$ (residual-g $g_s/g_0 \approx 10^{-6}$).

In Fig. 3 the corresponding fields are illustrated in the case $Pe_g = 1000$ ($g_s/g_0 \approx 10^{-5}$). In the absence of buoyancy convection (ideal zero-g situation), in the diffusion process after the removal of the diaphragm, a one-dimensional concentration distribution should develop with time toward both sides of the cell. In the presence of residual g natural convective flow arises and a single clockwise vortex cell appears in the middle of the cavity, with two small recirculation counter-clockwise vortex cells on the left and right sides (Fig. 2(a–b)). Buoyancy effects induced by the residual gravity accelerations are also responsible for distortions of the concentration field, compared to the diffusive situation (Fig. 2(c)). When the gravitational Peclet number (Pe_g) is increased the flow structure is not qualitatively changed, compared to the case of low Pe_g, but the velocities are larger (Fig. 3(a–b)). Consequently the isoconcentration lines are deformed by the flow and relevant distortions may be observed (Fig. 3(c)).

In Figs 4–6 the streamlines, the vector plots and the corresponding concentration distributions are illustrated in the case of g-jitters, in the absence of any residual gravity ($Pe_g = 0$), for three different values of the vibrational Peclet number ($Pe_v = 1000$, 10 000, 50 000, corresponding to g-jitters of the order of $g_\omega/g_0 \approx 3 \times 10^{-3}$, $g_\omega/g_0 \approx 10^{-2}$, $g_\omega/g_0 \approx 2 \times 10^{-2}$ at the frequency $f = 1$ Hz). According to previous studies on thermovibrational convection, when the solutal

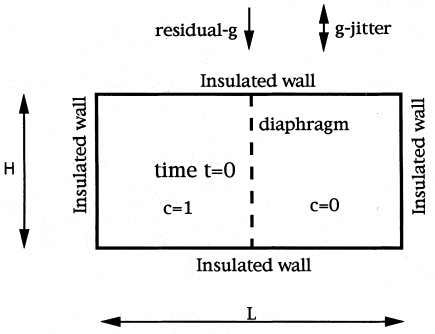

Fig. 1. Geometry of the problem, initial and boundary conditions.

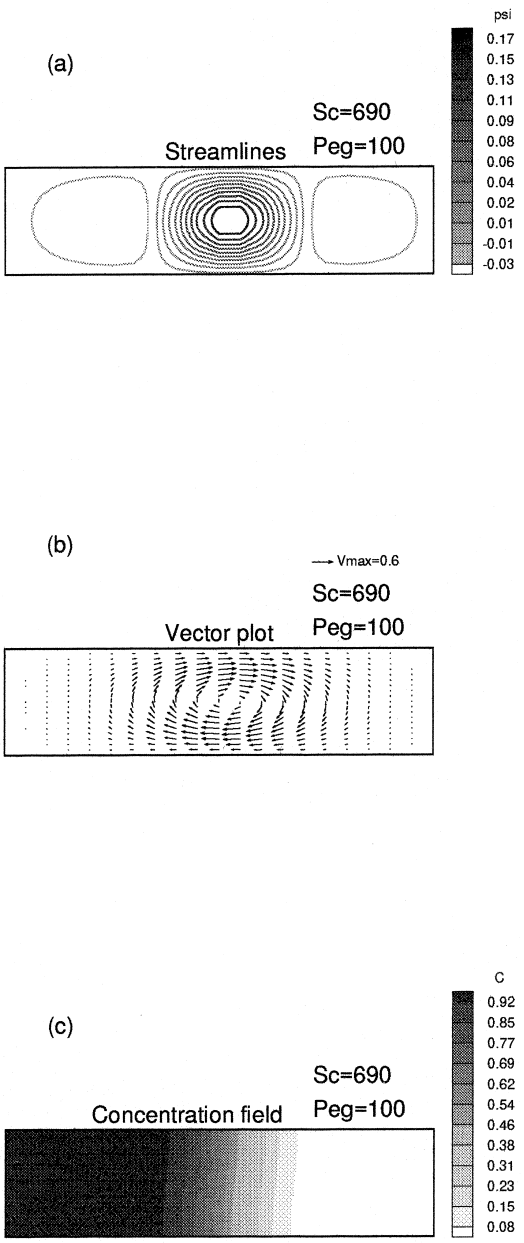

Fig. 2. Stream-lines (a), vector plots (b) and concentration field (c) for residual-g only without any g-jitter ($Pe_g = 100$ and $Pe_v = 0$). The maximum velocity is dimensionless.

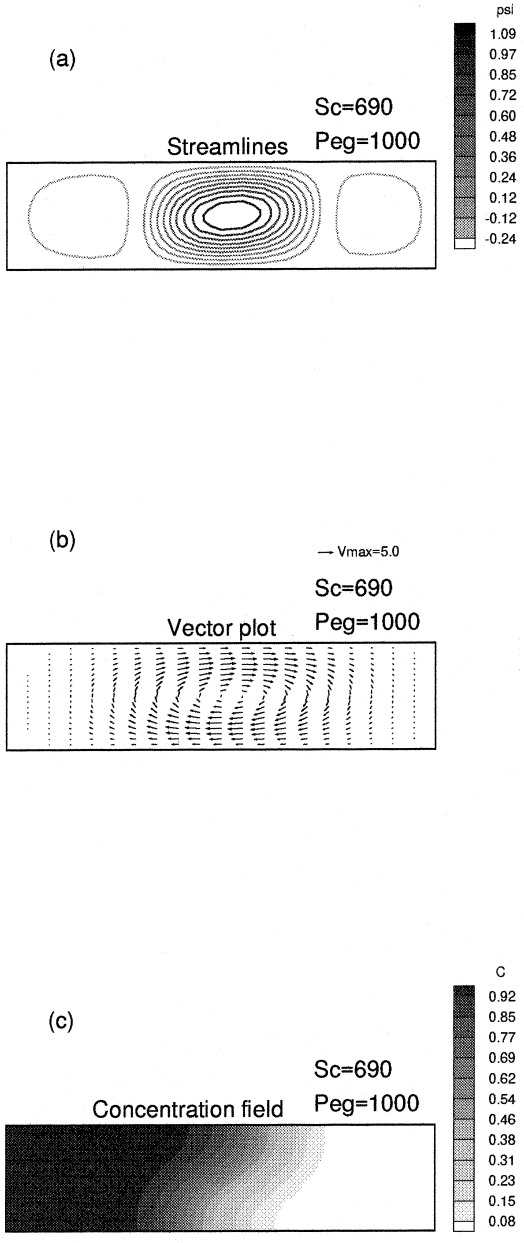

Fig. 3. Stream-lines (a), vector plots (b) and concentration field (c) for residual-g only without any g-jitter ($Pe_g = 1000$ and $Pe_v = 0$). The maximum velocity is dimensionless.

vibrational Peclet number is sufficiently small a steady stable regime with symmetric four vortex cells is established. The flow, mainly confined in the middle of the cavity where the concentration gradients are larger, is characterised by two pairs of vortex cells on the square diagonals, each with the same sign and intensity. In this case the concentration distortions, induced by the velocity field, are relatively small. When the solutal vibrational Peclet number increases above a critical value, this regime becomes unstable and there is a transition to a motion with a different structure. In Fig. 4 ($Pe_v = 1000$) the two clockwise cells (i.e. the top cell on the left and the bottom one on the right) are stronger than the others. For larger Pe_v numbers, the vibrational forces become more important and the coalescence of this pair of cells

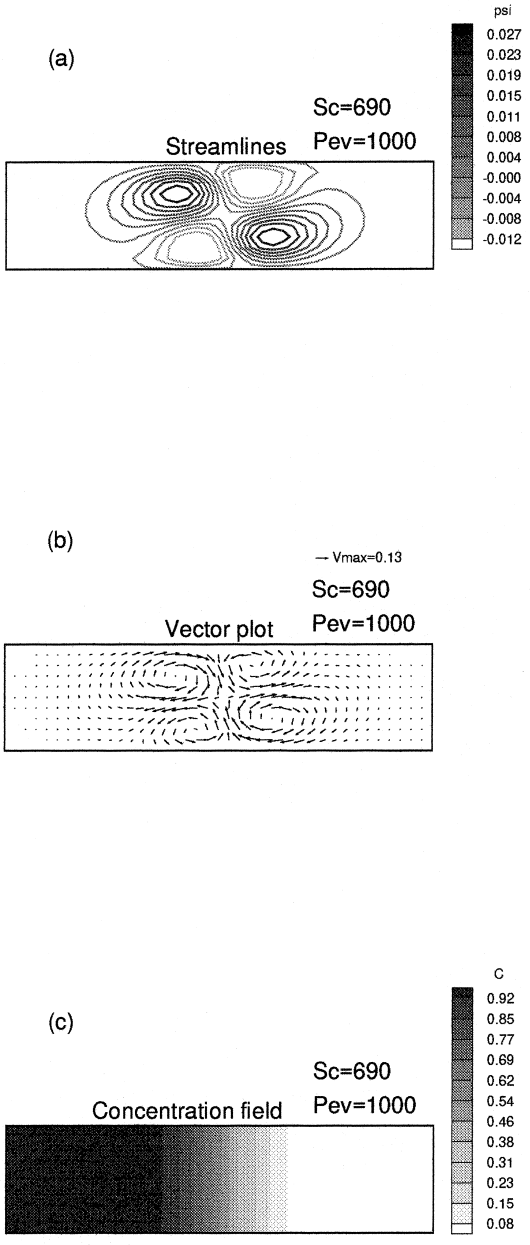

Fig. 4. Stream-lines (a), vector plots (b) and concentration field (c) for g-jitter only without any residual-g ($Pe_v = 1000$ and $Pe_g = 0$). The maximum velocity is dimensionless.

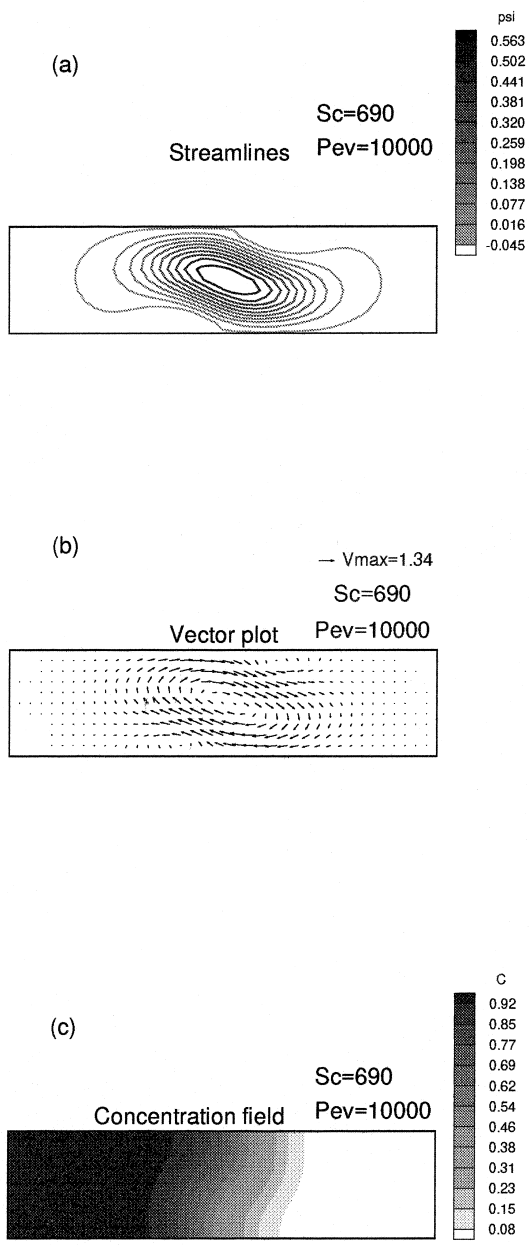

Fig. 5. Stream-lines (a), vector plots (b) and concentration field (c) for g-jitter only without any residual-g ($Pe_v = 10\,000$ and $Pe_g = 0$). The maximum velocity is dimensionless.

result in the development of a flow with bar (Figs 5(a–b), 6(a–b)).

The appearance of an asymmetry from a perfectly symmetrical system is confirmed by the stability analysis [10], that predicts a bifurcation of the four-vortex solution to a second asymmetric state, characterised by an elongated vortex cell along one or other of the diagonals, determined solely by the initial perturbations of the basic state, which play the role of the initial conditions. This asymmetry, confirmed by the numerical calculations, can be explained by truncation errors occurring during computer calculations, that introduce artificial small perturbations that are amplified under unstable conditions. In this situation the velocities increase and the con-

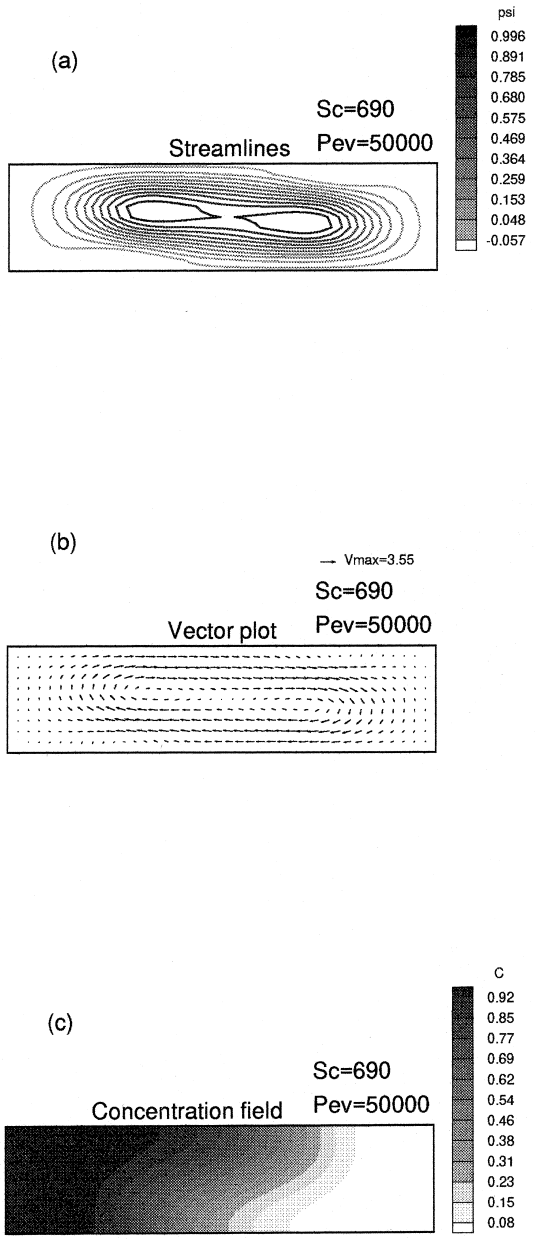

Fig. 6. Stream-lines (a), vector plots (b) and concentration field (c) for g-jitter only without any residual-g ($Pe_v = 50\,000$ and $Pe_g = 0$). The maximum velocity is dimensionless.

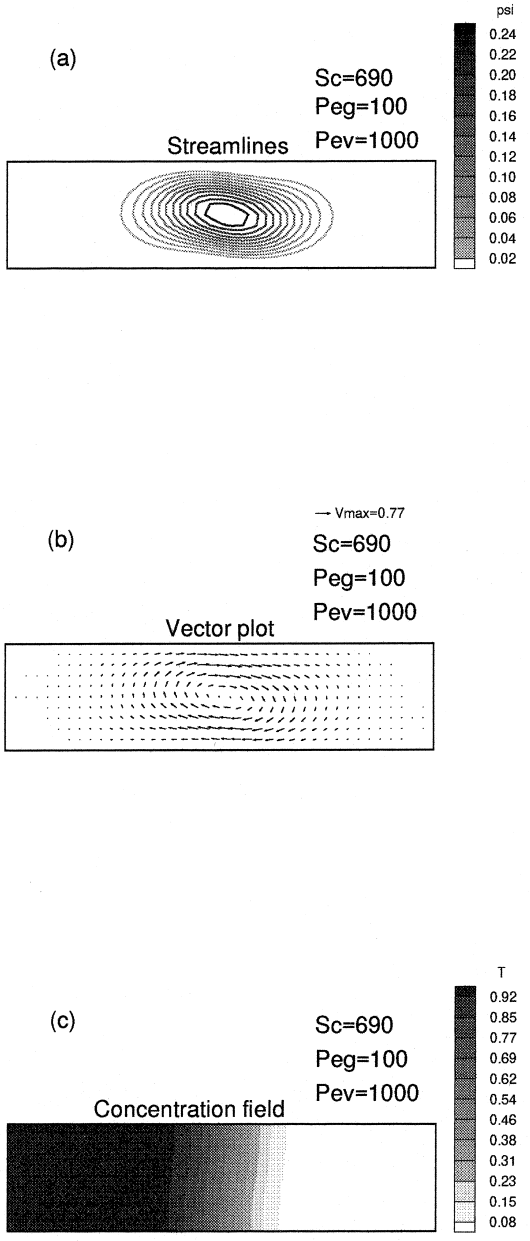

Fig. 7. Stream-lines (a), vector plots (b) and concentration field (c) for combined g-jitters and residual-g ($Pe_v = 1000$ and $Pe_g = 100$). The maximum velocity is dimensionless.

centration field is characterised by relevant distortions when compared to the purely diffusive situation.

The combined case resulting from steady residual g-levels superimposed to high frequency g-jitters is considered in Figs 7–9, where the flow fields corresponding to the case $Pe_g = 100$ are shown for three different values of Pe_v (1000, 10 000, 50 000). For lower values of Pe_v natural convection induced by residual-g prevails over the average vibrational effects and a single clock-wise vortex cell is observed in the middle of the cavity (Fig. 7(a–b)). When Pe_v increases, the vibrational convection becomes more important. Along the diagonal from the top-left to the bottom-right corners, where the effects due to residual-g and g-jitters are aiding, the circulation vortex cell is stronger, whereas two small counter-clock-

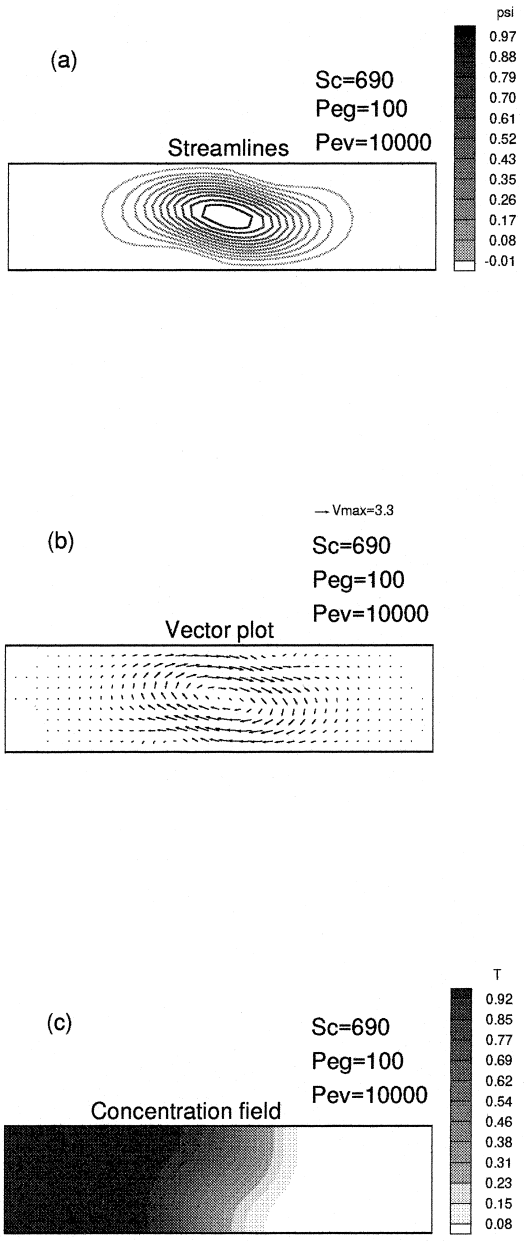

Fig. 8. Stream-lines (a), vector plots (b) and concentration field (c) for combined g-jitters and residual-g ($Pe_v = 10\,000$ and $Pe_g = 100$). The maximum velocity is dimensionless.

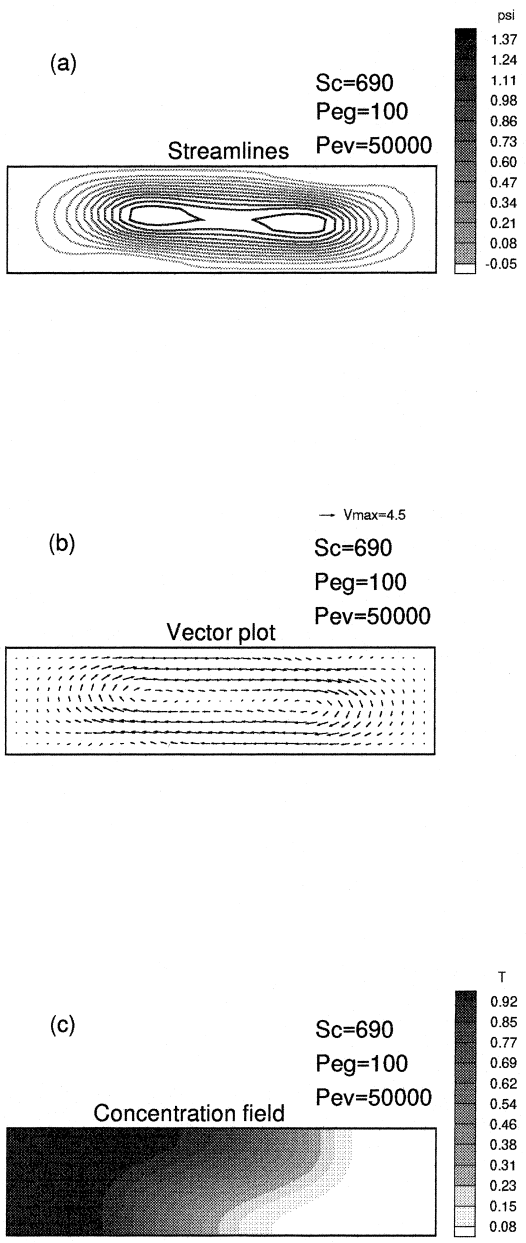

Fig. 9. Stream-lines (a), vector plots (b) and concentration field (c) for combined g-jitters and residual-g ($Pe_v = 50\,000$ and $Pe_g = 100$). The maximum velocity is dimensionless.

wise cells appear along the other diagonal (Fig. 8(a–b)). These behaviours are also confirmed by Fig. 9.

In conclusion, in the presence of residual-g, with or without g-jitter, the concentration field is clearly asymmetric, due to the asymmetry of the velocity field. When pure g-jitter is present, for sufficiently small values of the solutal vibrational Peclet number (say e.g. $Pe_v \leqslant 1000$), the velocity field is symmetric, and consequently the distribution of the iso-concentration contours is clearly symmetric. On the contrary, the concentration field becomes asymmetric for larger values of Pe_v, due to the bifurcation of the velocity field to an asymmetric solution.

When the concentration field is clearly asymmetric, interferometric techniques can be very useful to show the concentration distortions. However, it must be pointed out that many microgravity experiments deal with liquid

metals in furnaces at high temperatures, and that in these conditions the liquids are not accessible for optical diagnostic techniques.

All the results illustrated in Figs 2–9 have been obtained at the same value of the non dimensional time ($t = 0.1$). Since the process is time dependent, the flow pattern and the concentration fields change with time. However, the main features illustrated above do not change from a qualitative point of view. It must be pointed out that as the time increases the diffusion region becomes larger and the concentration gradients decrease, since the isoconcentration lines become more and more spaced out (see Fig. 10). Consequently, the convective cells become larger and larger, but the velocities decrease, until steady conditions are reached (with the concentration uniform everywhere in the cell and zero velocity). Figure 10 illustrates the behaviour at different times ($t = 0.1, 0.2, 0.3, 1.5$) in the case $Pe_v = 5000$.

In the present study the attention has been focused on the initial stage of the process ($t = 0.1$) since in this phase the density gradients are larger and it is obvious that better measurements of the diffusion coefficient are possible.

A numerical experiment has been performed to investigate the influence of the Schmidt number on the behaviour of the velocity and concentration regimes, in the range of interest for the applications ($Sc > 1$ for almost all fluids). It was found that the features of the flow and concentration fields remain practically unchanged from a qualitative point of view. However, varying the Schmidt number, for prescribed values of the solutal Peclet numbers, the computed velocities exhibit an interesting behavior during the transient process. This is illustrated in Fig. 11,, where the maximum dimensionless velocity is reported vs. Sc at different times, in the case $Pe_v = 10\,000$. For sufficiently small values of the non dimensional time (corresponding to the initial stage of the process, when the density gradients are particularly large) the maximum velocity is initially an increasing function of Sc. Since larger flow velocities imply a more rapid diffusion, this leads to a more rapid decrease of the concentration gradient, so that the profile of the maximum velocity reaches a maximum at a certain value of Sc and then decreases. The value of Sc at which the peak occurs depends on the value of the non dimensional time. When t increases this peak occurs at smaller values of Sc, until a decreasing behaviour is found for any Sc. This is justified by the fact that the characteristic non dimensional time of the transient diffusion process is a decreasing function of Sc, so that at the same times (sufficiently large) the level of the residual convection decreases with Sc.

Moreover Fig. 11 shows that, at each time t, the velocities reach an asymptotic value for large values of Sc ($Sc > 10$). This result can be explained by an asymptotic analysis of the dimensionless equations (33)–(38). In particular, when the Schmidt number is rather high, the inertial terms in the equations (34), (35) become small compared to the driving and to the viscous terms so that the non dimensional problem only weakly depends on the Schmidt number.

Thus, the results of the present study, obtained for the particular value of $Sc = 690$, that is a representative of a class of microgravity experiments (binary mixtures of salt in water) very sensitive to g-disturbances, can be generalized to many other fluids with large Schmidt numbers.

5.2. Time-profiles of concentration distortions

The interest of a typical diffusion experiment is mainly related to the transient phase of the phenomenon, because the diffusion coefficient is obtained by observing the time variation of the average concentrations. For this reason we have computed the transient profiles of the concentration distortions (at the same time corresponding to the results of Figs 2–9, i.e. $t = 0.1$). A possible definition of the distortions, measuring the difference between the real concentration fields, in presence of residual accelerations and g-jitters, and the ideal purely diffusive field, may be introduced as:

$$\varepsilon_c = \max(c - c_{diff})/\Delta c$$

where c_{diff} is the concentration in the diffusive situation and max denotes the maximum value in the computational domain.

In Fig. 12 the concentration distortions have been reported as functions of time for different Pe_g numbers in the case $Pe_v = 0$ (Fig. 12(a)), for different Pe_v numbers in the case $Pe_g = 0$ (Fig. 12(b)) and for different Pe_v numbers in the case $Pe_g = 100$ (Fig. 12(c)). In the first case, when only residual g-levels effects are considered, the distortions gradually increase with time and, after a maximum, they decrease very slowly (Fig. 12(a)). In the case of vibrational convection induced by g-jitters (Fig. 12(b)) the concentration distortions reach a maximum very soon, because at the beginning of the diffusion process the isoconcentration lines are all confined in the middle of the cavity and the average vibrational convective effects, proportional to the square of the concentration gradients are responsible for the larger velocities. As a consequence, the concentration field at the beginning is significantly deformed compared to the ideal purely diffusive field. As the time increases the diffusion spreads far away towards the left and right sides, the concentration field becomes more and more developed until the final steady state is reached and the flow field vanishes.

In the case of combined effects resulting from residual-g superimposed to g-jitters, for low solutal vibrational Peclet numbers the typical behaviour associated to the natural convection is observed and the concentration distortions gradually increase in the first phase and

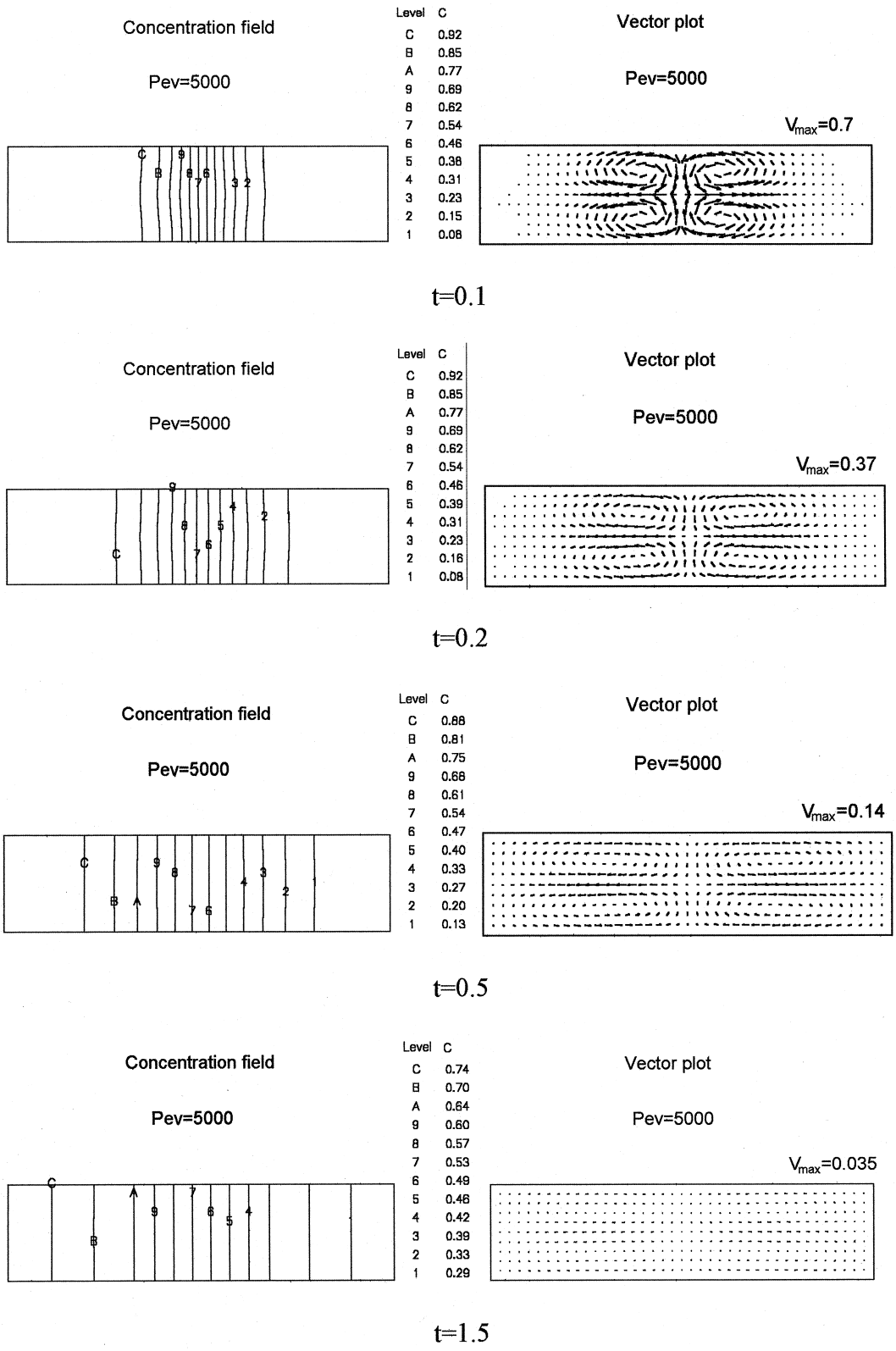

Fig. 10. Vector plots and concentration field for $Pe_v = 5000$ and $Pe_g = 0$, at different times. The maximum velocity is dimensionless.

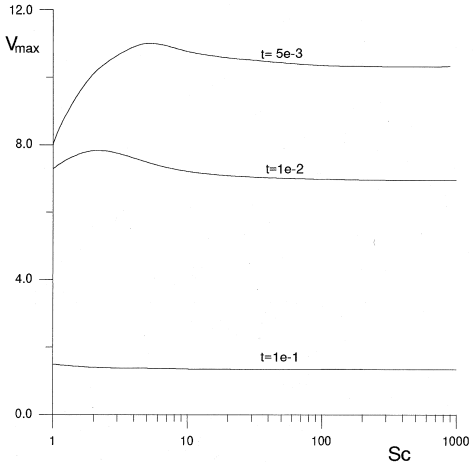

Fig. 11. Maximum computed non dimensional velocity vs. Sc at different times, for $Pe_v = 10\,000$ and $Pe_g = 0$.

decrease in the second phase of the process. For higher Pe_v number the effects due to g-jitters prevail and the distortions reach a maximum value very soon and then decrease. In conclusion we may say that g-jitters may have relevant effects during the unsteady process, particularly in the initial transient phase when the concentration and flow field begin to develop, far from the asymptotical behaviour corresponding to steady state.

5.3. Cross-average concentration profiles and percentage errors

The fluid-dynamic model allows to evaluate convective effects associated to residual-g and g-jitters and to determine the distortions of the concentration field with respect to the ideal zero-g field. These distortions are responsible for errors in the measurement of the diffusion coefficient. In a one-dimensional purely diffusive process, the solution of the time-dependent species equation gives the following time and space dependence of the longitudinal concentration gradient:

$$\frac{\partial c}{\partial x}(x,t) = -1/\sqrt{\pi D t}\exp(-(x-L/2)^2/4Dt. \tag{44}$$

In a quasi one-dimensional situation one can define an average cross-sectional concentration along the section of height H:

$$C(x,t) = 1/H\int_0^H c(x,y,t)\,\mathrm{d}y. \tag{45}$$

If the longitudinal profile of the average concentration gradient $\partial c/\partial x(x,t)$, at a given time, is interpolated with the exponential law (44), the percentage error in the measurement of the diffusive coefficient, due to the convection, is defined by $P_{err} = (D - D_{diff})/D_{diff}$, where D is obtained by the best fit of the profile obtained in presence of g-disturbances and D_{diff} is the correct value of the diffusion coefficient corresponding to the purely one-dimensional diffusive situation.

In Fig. 13 the cross-section average concentration gradients along x-coordinate are shown for different Pe_v in the case $Pe_g = 0$ (Fig. 13(a)) and $Pe_g = 100$ (Fig. 13(b)). In Fig. 14 the maximum concentration distortions and the corresponding percentage errors in the measurement of the diffusion coefficient are shown vs. Pe_g for $Pe_v = 0$ (Fig. 14(a)), vs. Pe_v for $Pe_g = 0$ (Fig. 14(b)) and vs. Pe_v for $Pe_g = 100$ (Fig. 14(c)). In particular, the comparison between the cross-average concentration gradients obtained for $Pe_v = 10\,000$ with and without residual-g (Fig. 15(c)) shows that a residual-g of the order of magnitude of $g_s/g_0 \approx 10^{-6}$ is responsible for negligible percentage error in the measurement of the diffusion coefficient, whereas more relevant distortions could be associated to extremely large g-jitters.

6. Conclusions

The effects of g-disturbances on typical microgravity experiments for the measurement of the diffusion coefficients in liquids have been investigated by numerical solutions of the time-averaged field equations including both buoyancy and vibrational driving actions.

The transient velocity and concentration distributions, the time profiles of the concentration distortions and the percentage errors in the measurement of the diffusion coefficient have been obtained for different solutal gravitational Peclet numbers (Pe_g) for residual-g only without any g-jitter ($Pe_v = 0$), for different solutal vibrational Peclet numbers (Pe_v), for g-jitters only without residual-g ($Pe_g = 0$), and in the combined case of simultaneous residual-g and g-jitters.

The main characteristics of the flow fields and of the concentration distributions have been presented and discussed with particular emphasis to the influence of the average vibrational convective effects associated to g-jitters, and some important conclusions have been outlined. In particular it has been pointed out that the flow field organisations and the time-profiles of the thermo-fluid-dynamic distortions are very different in the two cases of natural convection (residual-g) and vibrational convection (g-jitters). G-jitters may have relevant effects during the initial transient phase when the concentration and flow field begin to develop, so that the concentration distortions, as functions of time, reach a maximum value very soon and then decrease. The numerical computations pointed out that a residual-g of the order of magnitude of $g_s/g_0 \approx 10^{-6}$ is responsible for a negligible error in the measurement of the diffusion coefficient, whereas more relevant distortions could be associated to extremely large g-jitters.

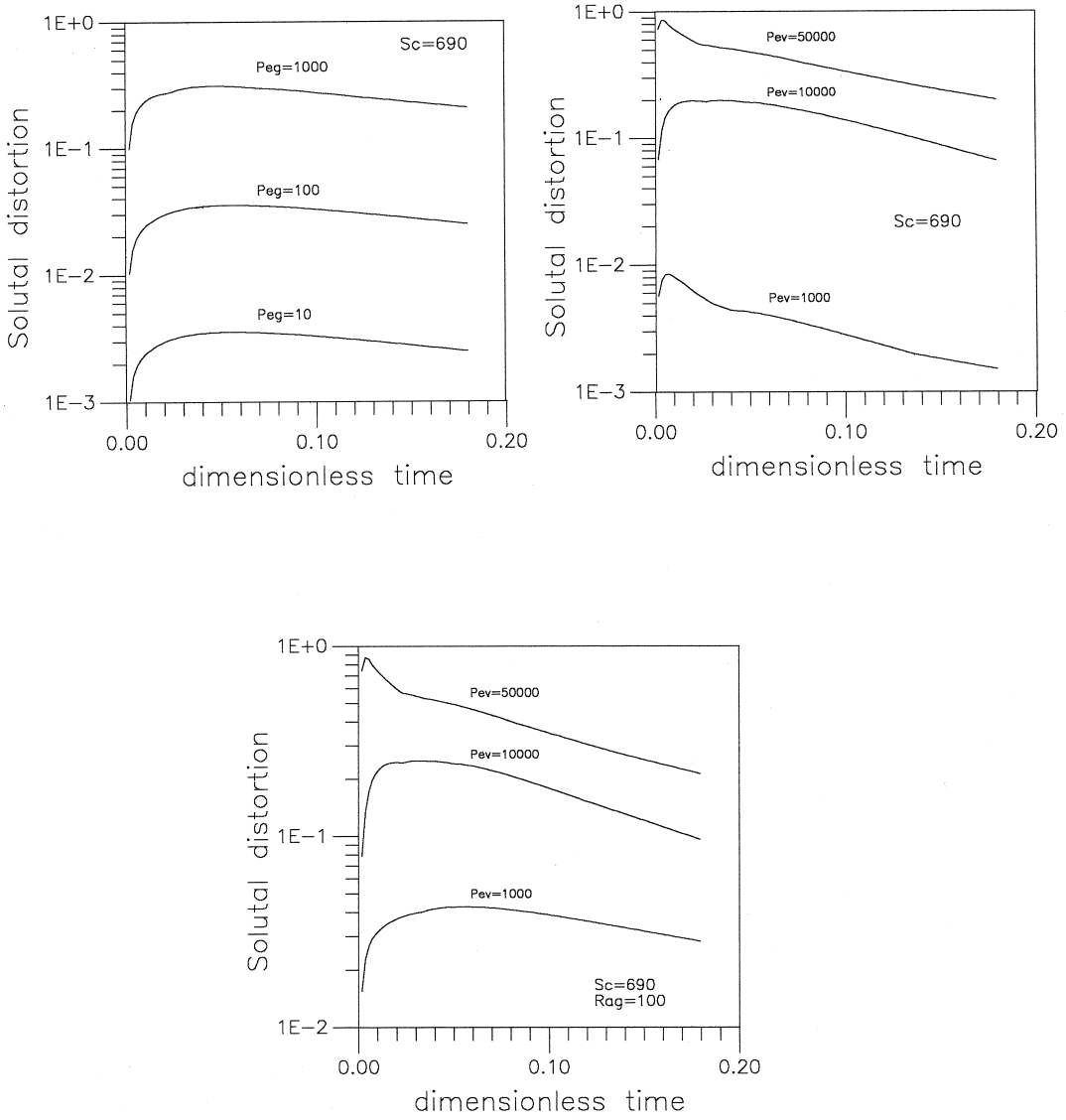

Fig. 12. Concentration distortions as functions of time for different gravitational Peclet numbers in the case $Pe_v = 0$ (a), for different vibrational Peclet numbers in the case $Pe_g = 0$ (b), and for different vibrational Peclet numbers for $Pe_g = 100$ (c).

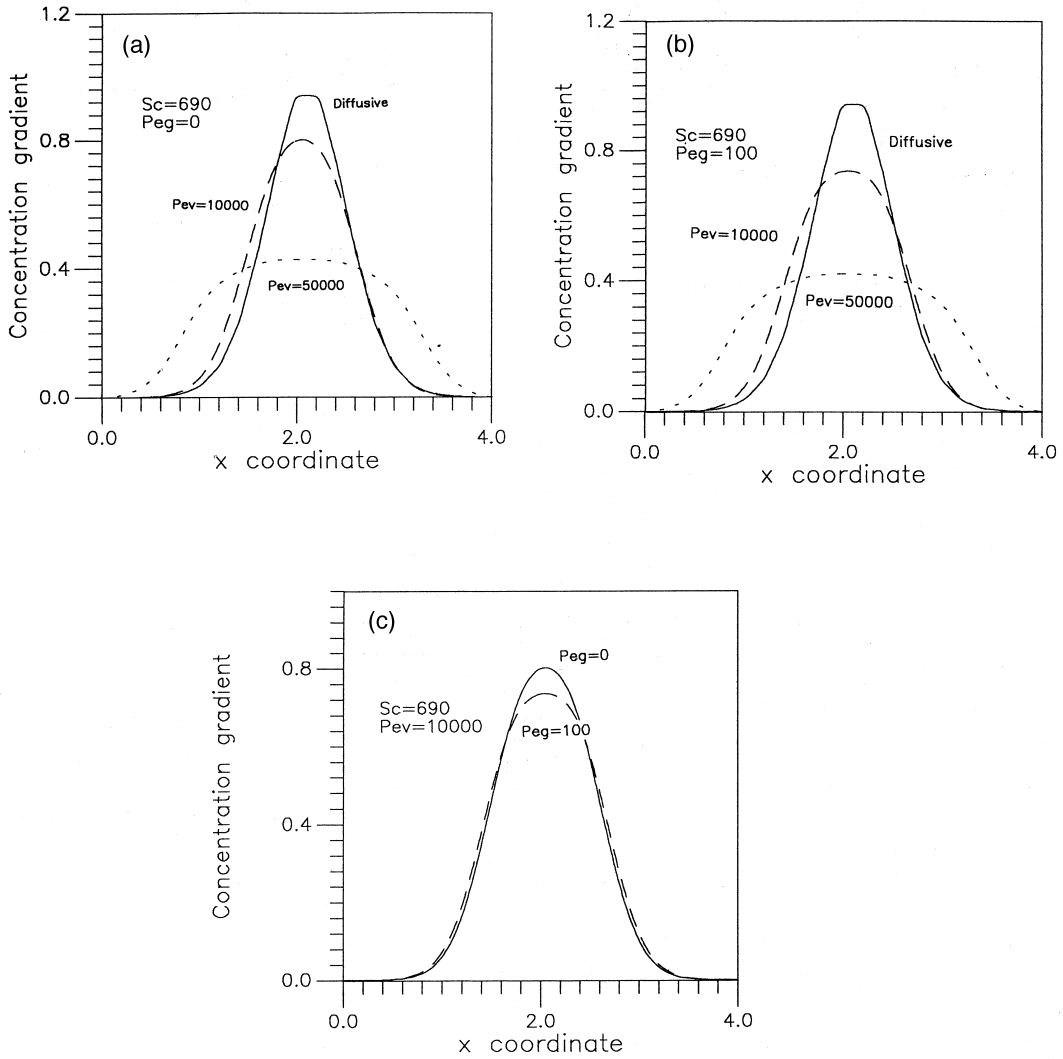

Fig. 13. Cross-section average concentration gradients along x-coordinate for different vibrational Peclet numbers for $Pe_g = 0$ (a), and for $Pe_g = 100$ (b). Comparison between the average concentration gradients obtained in the case $Pe_v = 10\,000$ with and without residual-g (c).

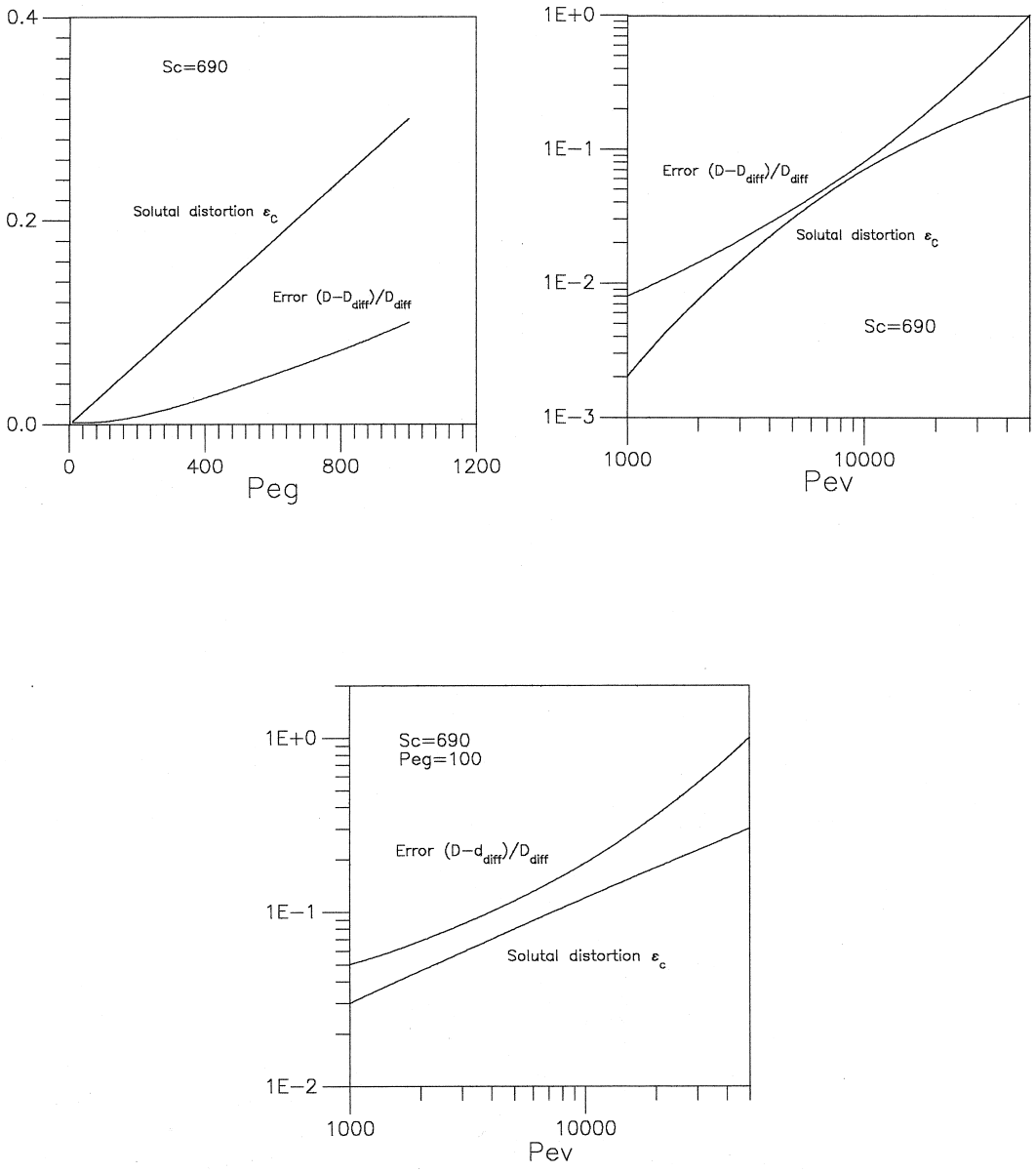

Fig. 14. Concentration distortions and percentage error in the measurement of the diffusion coefficient as functions of the gravitational Peclet number (Pe_g) in the case $Pe_v = 0$ (a), of the vibrational Peclet number (Pe_v) in the case $Pe_g = 0$ (b), and of the vibrational Peclet number (Pe_v) in the case $Pe_g = 100$ (c).

Although the theoretical formulation developed in the first part of the paper includes both concentration and temperature fields, the particular case considered in the calculations deal with the problem of concentration diffusion in an isothermal system, so that cross coupling effects between the temperature and the concentration fields have not been investigated. The authors intend to consider this aspect in a forthcoming paper devoted also to measurement of Soret coefficients.

Acknowledgement

The support of this study by the European Space Agency, under contract N.22054/94/F/FL, is gratefully acknowledged.

References

[1] W. Knabe, D. Eilers, Low-gravity environment in spacelab, Acta Astronaut 9 (1992) 187.
[2] H. Hamacher, B. Fitton, J. Kingdom, The environment of Earth-Orbiting systems, in: H.U. Walter (Ed.), Fluid Sciences and Material Sciences in Space, Springer-Verlag, 1987, pp. 1–50.
[3] M.J.B. Rogers, R. DeLombard, Summary report of mission acceleration measurements for STS-65, NASA Technical Memorandum 106 871, 1995.
[4] Y. Malmejac, G. Frohberg, Mass transport by diffusion, in: H.U. Walter (Ed.), Fluid Sciences and Material Sciences in Space, Springer-Verlag, 1987, pp. 159–190.
[5] D. Thevenard, H. Ben Hadid, Low Prandtl number convection in a rectangular cavity with longitudinal thermal gradient and transverse *g*-jitters, Int. J. Heat Mass Transfer 34 (8) (1991) 2167–2173.
[6] T.C. Jue, B. Ramaswamy, Natural convection with thermocapillary and gravity modulation effects in low-gravity environments, J. Spacecr. Rockets 29 (1992) 856.
[7] J. Alexander, S. Amiroudine, J. Ouazzani, F. Rosenberger, Analysis of the low gravity tolerance of Bridgman–Stockbarger crystal growth II. Transient and periodic accelerations, J. Cryst. Growth 113 (1991) 21.
[8] Y. Kamotani, A. Prasad, S. Ostrach, Thermal convection in an enclosure due to vibrations aboard a spacecraft, AIAA J. 19 (1981) 511.
[9] P.D. Richardson, Effects of sound and vibrations on heat transfer, Appl. Mech. Rev. 20 (1967) 201–217.
[10] G.Z. Gershuni, E.M. Zhukhovitsky, Vibrational thermal convection in zero-gravity, Fluid Mech.—Sov. Res. 15 (1986) 63–84.
[11] R. Monti, R. Savino, A new approach to *g*-level tolerability for fluid and material science experiments, Acta Astronautica 37 (1994) 313–331.
[12] R. Monti, R. Savino, The basis and the recent developments of Napolitano's scaling and order of magnitude analysis, Microgravity Quarterly 5 (1) (1995) 13–17.
[13] Highlights of the International Workshop on non-gravitational mechanisms of convection and heat/mass transfer, Zvenigorod, Russia, September 1994, Guest Editor G.Z. Gershuni, Microgravity Quarterly 4 (4) (1994).
[14] W.S. Fu, W.J. Shieh, A study of thermal convection in an enclosure induced simultaneously by gravity and vibration, Int. J. Heat Mass Transfer 35 (7) (1992) 1695–1710.
[15] W. Uspenskii, J.J. Favier, High frequency vibration and natural convection in Bridman-scheme crystal growth, Int. J. Heat Mass Transfer 37 (4) (1994) 691–698.
[16] V.I. Chenrnatynski, G.Z. Gershuni, R. Monti, R. Savino, Transient effects of *g*-pulses in a fluid cell heated from below, Microgravity Quarterly 5 (3) (1995) 152–161.
[17] R. Monti, R. Savino, Microgravity experiments acceleration tolerability on space orbiting laboratories, Journal of Spacecraft and Rockets 33 (5) (1996) 707–716.
[18] R. Monti, R. Savino, Influence of *g*-jitter on fluid physics experimentation on-board the International Space Station, Symposium Proceedings on 'Space Station Utilisation', Darmstadt, Germany, 30 September–2 October 1996, ESA-SP-385, pp. 215–224.
[19] R. Monti, Gravity jitters: effects on typical fluid science experiments, in: N. Koster, R.L. Sani (Eds.), Low-Gravity Fluid Dynamics and Transport Phenomena; Progress in Astronautics and Aeronautics 130 (1990) 275–307.
[20] W. Littke, Diffusion controlled growth of single crystals of protein. Summary review of Sounding Rockets Experiments in Fluid Science and Material Science, ESA SP 1132 1 (1991) 204–205.
[21] W. Littke, C. John, Protein single crystal growth under microgravity, Science 225 (1992) 203–204.
[22] R. Bosch, P. Lautenschlager, L. Potthast, J. Stapleman, Experiment equipment for protein crystallization in microgravity facilities, Journal Crystal Growth 122 (1992) 310.
[23] L.G. Napolitano, Surface and buoyancy driven free convection, Acta Astronautica 9 (1982) 199.
[24] L.G. Napolitano, A. Viviani, R. Savino, Double-diffusive dissipative layers along vertical free surfaces, Int. J. Heat and Mass Transfer 35 (5) (1992) 1003–1025.